OXFORD

Human Molecular Genetics, 2015, Vol. 24, No. 24 6886–6898

doi: 10.1093/hmg/ddv389
Advance Access Publication Date: 18 September 2015
Original Article

ORIGINAL ARTICLE

Fragile X protein mitigates TDP-43 toxicity by remodeling RNA granules and restoring translation

Alyssa N. Coyne[1,2], Shizuka B. Yamada[1], Bhavani Bagevalu Siddegowda[1], Patricia S. Estes[1], Benjamin L. Zaepfel[1], Jeffrey S. Johannesmeyer[1], Donovan B. Lockwood[1,2], Linh T. Pham[1], Michael P. Hart[4], Joel A. Cassel[5], Brian Freibaum[6], Ashley V. Boehringer[1,2,3], J. Paul Taylor[6], Allen B. Reitz[5], Aaron D. Gitler[4] and Daniela C. Zarnescu[1,2,3,*]

[1]Department of Molecular and Cellular Biology, [2]Department of Neuroscience, [3]Department of Neurology, University of Arizona, Tucson, AZ, USA, [4]Department of Genetics, Stanford University School of Medicine, Stanford, CA, USA, [5]ALS Biopharma, LLC, Doylestown, PA, USA and [6]Department of Neurobiology, St. Jude Children's Research Hospital, Memphis, TN, USA

*To whom correspondence should be addressed. Email: zarnescu@email.arizona.edu

Abstract

RNA dysregulation is a newly recognized disease mechanism in amyotrophic lateral sclerosis (ALS). Here we identify Drosophila fragile X mental retardation protein (dFMRP) as a robust genetic modifier of TDP-43-dependent toxicity in a Drosophila model of ALS. We find that dFMRP overexpression (dFMRP OE) mitigates TDP-43 dependent locomotor defects and reduced lifespan in Drosophila. TDP-43 and FMRP form a complex in flies and human cells. In motor neurons, TDP-43 expression increases the association of dFMRP with stress granules and colocalizes with polyA binding protein in a variant-dependent manner. Furthermore, dFMRP dosage modulates TDP-43 solubility and molecular mobility with overexpression of dFMRP resulting in a significant reduction of TDP-43 in the aggregate fraction. Polysome fractionation experiments indicate that dFMRP OE also relieves the translation inhibition of *futsch* mRNA, a TDP-43 target mRNA, which regulates neuromuscular synapse architecture. Restoration of *futsch* translation by dFMRP OE mitigates Futsch-dependent morphological phenotypes at the neuromuscular junction including synaptic size and presence of satellite boutons. Our data suggest a model whereby dFMRP is neuroprotective by remodeling TDP-43 containing RNA granules, reducing aggregation and restoring the translation of specific mRNAs in motor neurons.

Introduction

Amyotrophic lateral sclerosis (ALS) is a progressive neurodegenerative disease that affects upper and lower motor neurons and typically leads to death within 2–5 years after diagnosis (1). Familial ALS (fALS) accounts for approximately 10% of cases, with the remaining 90% being sporadic (sALS) and poorly understood. The most common cause of fALS is a GGGGCC repeat expansion in *C9ORF72* whose potential disease mechanisms comprise haploinsufficiency, RNA dysregulation and RAN translation (2). Other loci linked to fALS and sALS include TAR DNA-binding protein (TDP-43), SOD1, alsin, senataxin, VAMP/synaptobrevin-associated protein, dynactin, angiogenin, Fused in Sarcoma (FUS), ataxin 2, and profilin 1 (3). Based on the known functions of these genes, ALS appears to result from defects in multiple cellular processes including oxidative stress, intracellular transport and RNA metabolism among others (3,4).

Received: July 30, 2015. **Revised and Accepted:** September 14, 2015

With the recent discoveries of RNA foci containing expanded GGGGCC repeats as well as mutations in several RNA binding proteins (e.g. TDP-43, FUS), new hypotheses have emerged in the field, suggesting a central role for RNA dysregulation in the pathophysiology of the disease (5). Of the known RNA binding proteins involved, TDP-43 is both a causative factor and also associates with pathological aggregates in a vast majority of ALS cases, regardless of etiology (6–10). Mutations in TDP-43 have been linked to both fALS and sALS and have been shown to increase its propensity for aggregation (11). Notably, studies in several animal models indicate that alterations in TDP-43 expression result in several phenotypes reminiscent of ALS pathology including locomotor dysfunction and reduced survival (12–20). Taken together, these findings suggest that TDP-43 is a critical contributor to ALS and thus understanding both its normal function as well as its involvement in pathophysiology is likely to provide important insights for developing effective therapeutic strategies.

TDP-43 has been shown to regulate multiple aspects of RNA metabolism and most recently has been implicated in the transport and translational regulation of specific mRNA targets (21,22). TDP-43 contains nuclear localization (NLS) and export signals (NES), two RNA recognition motifs (RRM1 and RRM2), and a glycine-rich, prion-like, C-terminal domain (23–25). The RRM1 domain is required for toxicity *in vivo* (26,27) providing evidence that TDP-43's regulation of RNAs is essential for disease pathogenesis.

TDP-43 has also been shown to associate with other RNA binding proteins that function as splicing or translational regulators (28). In cultured neurons, TDP-43 colocalizes with Fragile X protein (FMRP) and Staufen in RNA granules in an activity-dependent manner (29–31). In addition, TDP-43 has been shown to associate with stress granules (SG) that sequester mRNAs and inhibit their translation during environmental stress (32–35). Although TDP-43 does not seem to be required for SG formation, ALS linked mutations in TDP-43 were shown to alter the dynamics of SG (33). This is consistent with our previous findings that the molecular mobility of wild-type TDP-43 differs from that of the mutant variants in primary motor neurons (36). These data lend support to the notion that TDP-43's toxicity is linked to the presence of SG. Furthermore, it has been shown that TDP-43 containing cytoplasmic aggregates can 'evolve' from paraquat induced SG (37). Together, these findings suggest a scenario whereby, in response to stress, possibly caused by aging or other environmental factors, TDP-43 localizes to cytoplasmic SG that lead to altered ribostasis and have the potential to mature into cellular aggregates similar to those associated with ALS pathology (38–40).

We have previously shown that expression of TDP-43 in Drosophila motor neurons or glia recapitulates several aspects of ALS pathology (14,36). Here we use this Drosophila model to probe the ribostasis hypothesis and identify functional neuroprotective partners of TDP-43. In taking a candidate RNA binding protein approach we found that Drosophila fragile X mental retardation protein (dFMRP), a known translational regulator linked to synaptic deficiency and cognitive dysfunction (41), modulates the toxicity of TDP-43 *in vivo*. dFMRP loss of function enhances TDP-43 phenotypes while dFMRP overexpression (dFMRP OE) mitigates TDP-43-dependent neurodegeneration, locomotor dysfunction and reduced survival. TDP-43 colocalizes with dFMRP in neuronal RNA granules, some of which are positive for the SG marker polyA binding protein (PABP). Furthermore, immunoprecipitation experiments indicate that TDP-43 and fragile X mental retardation protein (FMRP) form a complex in flies and human cells. Using a combination of cellular fractionations and fluorescence recovery after photobleaching (FRAP) we show that dFMRP modulates the solubility of TDP-43 and its association with aggregates as well as its molecular mobility within neurites. Quantification of transcript and protein levels together with polysome fractionation experiments show that TDP-43 associates with both the non-translated RiboNuclearProtein particles (RNPs) and actively translating ribosomes, and regulates the translation of specific mRNA targets. Taken together, fractionation and polysome profiling experiments suggest that dFMRP OE remodels TDP-43 containing RNP granules and restores the translation of specific mRNA targets such as *futsch*, which in turn alleviates TDP-43-dependent neuromuscular synapse morphological phenotypes. These findings suggest RNA granule remodeling and translation restoration as potential targets for the development of therapeutic strategies in ALS.

Results

dFMRP is a potent modifier of TDP-43 neurotoxicity *in vivo*

Given the involvement of TDP-43 in various aspects of RNA metabolism, we used a candidate approach to identify RNA binding proteins that could modulate TDP-43 toxicity. We have previously shown that expression of human TDP-43 (wild-type or ALS linked mutations) in the eye neuroepithelium results in age dependent neurodegeneration as indicated by a depigmentation phenotype (14,36) (compare Fig. 1A and D to Fig. 1G). Here we report that dFMRP, an established translational regulator and component of neuronal RNA granules, modulates TDP-43-dependent neurotoxicity *in vivo*. Using the eye-specific GMR Gal4 driver we co-expressed TDP-43 and a dFMRP RNAi knock-down construct ($FMRP^{RNAi}$, see 42) and found an enhancement of the neurodegenerative phenotype caused by TDP-43 alone (compare Fig 1B and E to Fig. 1A and D). We also performed this experiment using a null allele of dFMRP ($dfmr1^{50M}$) and found a similar enhancement when dFMRP levels were reduced by 50% in the context of TDP-43 expression (Supplementary Material, Fig. S2A–F). Conversely, dFMRP OE in the eye robustly suppressed TDP-43 induced neurodegeneration, (compare Fig. 1C and F to Fig. 1A and D). Notably, $dFMRP^{RNAi}$, and dFMRP OE, did not cause depigmentation phenotypes on their own (Fig. 1G–I). Importantly, the effects of dFMRP dosage on TDP-43 mediated toxicity were not a result of Gal4 dilution resulting from the addition of a second UAS element (Supplementary Material, Fig. S1A–F). Furthermore, TDP-43 protein and mRNA levels were not altered by dFMRP indicating that neuroprotective effects do not occur by altering TDP-43 expression (Supplementary Material, Fig. S4). Albeit qualitative, these genetic interactions demonstrate that TDP-43 functions *in vivo* with dFMRP, and that TDP-43 neurotoxicity is sensitive to FMRP dosage.

Next we sought to determine whether TDP-43 and dFMRP also exhibit functional interactions in motor neurons. To test this, we used larval turning assays, a measure of locomotor function, which we previously found to be impaired by TDP-43 overexpression (14,36). Using the D42 Gal4 motor neuron driver we co-expressed TDP-43 with either $dFMRP^{RNAi}$ or dFMRP OE. Larval turning assays demonstrated that a reduction in dFMRP levels leads to an enhancement of locomotor dysfunction while overexpression of dFMRP suppresses TDP-43-dependent locomotor defects (Fig. 1J and K). Note that alterations in locomotor function were not due to the addition of a second UAS element (Supplementary Material, Fig. S1G) and as with $dFMRP^{RNAi}$, a null allele of dFMRP ($dfmr1^{50M}$) also caused a statistically significant

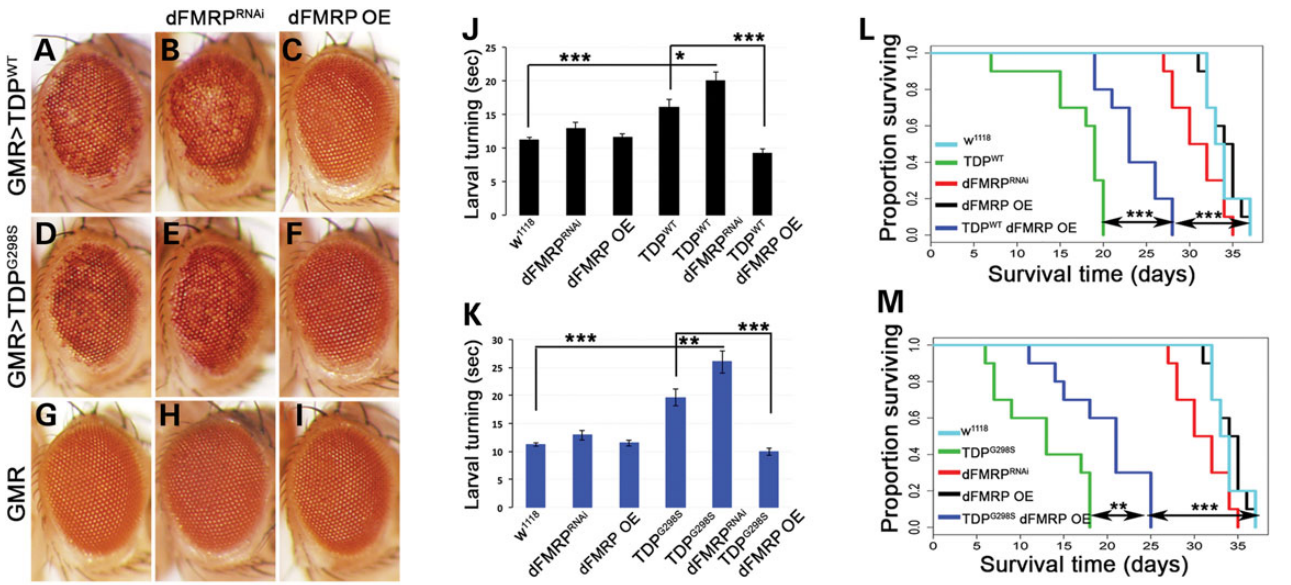

Figure 1. dFMRP modulates the neurotoxicity caused by TDP-43 *in vivo*. (**A–I**) GMR Gal4 expression of TDP-43 variants: WT (A) and G298S (D), results in depigmentation, which is enhanced by dFMRP knock-down (dFMRP^{RNAi}; B and E) and suppressed by dFMRP overexpression (dFMRP OE; C and F) compared to controls (G–I). (**J** and **K**) D42 Gal4 expression of TDP-43 variants WT (J) and G298S (K), results in increased larval turning time, which is exacerbated by dFMRP^{RNAi} and rescued by dFMRP OE. (**L** and **M**) D42 Gal4 expression of TDP-43 variants WT (L) and G298S (M) results in reduced adult survival time, which is rescued by dFMRP OE. dFMRP^{RNAi} shifts the lethality caused by TDP-43 to pupal stage (see text).

enhancement of TDP-43 mediated locomotor dysfunction (Supplementary Material, Fig. S2G). Thus, as in the retina, dFMRP is a potent modifier of TDP-43 neurotoxicity in motor neurons, as indicated by quantitative locomotor function assays. Interestingly, when Drosophila TDP-43, TBPH, is reduced by RNAi knock-down (TBPH^{RNAi}), dFMRP OE does not rescue locomotor dysfunction (Supplementary Material, Fig. S3). This indicates that TDP-43 expression is required for the neuroprotective effects of dFMRP and suggests that toxicity caused by loss of TBPH occurs through a distinct mechanism.

We also found that dFMRP OE leads to a statistically significant increase in adult survival time (28 days for TDP^{WT} dFMRP OE compared to 20 days for TDP^{WT}, $P_{value} = 0.0003$, Fig. 1L, and 25 days for TDP^{G298S} dFMRP OE compared to 18 days for TDP^{G298S}, $P_{value} = 0.005$, Fig. 1M). Notably, this increase in lifespan was not due to a Gal4 dilution effect caused by the presence of a second UAS element (Supplementary Material, Fig. S1H) highlighting the ability of dFMRP to modulate TDP-43 toxicity in multiple assays. In contrast, dFMRP knock-down in the context of TDP-43 overexpression resulted in 100% lethality at the pupal stage. Compared to controls, neither dFMRP knock-down by RNAi nor dFMRP OE have a significant effect on lifespan (35 days for dFMRP^{RNAI}, 37 days for both dFMRP OE and w^{1118}, $P_{value} = 0.06$ and 0.9, respectively). These findings indicate that TDP-43-dependent phenotypes including neurodegeneration, locomotor function and lifespan are modulated by dFMRP dosage, with dFMRP upregulation being robustly neuroprotective.

TDP-43 and dFMRP colocalize with PABP in neuronal RNA granules

It has been previously reported that TDP-43 and FMRP colocalize in the somatodendritic compartment of cultured mammalian neurons, in an activity-dependent manner (29–31). Given these published data and our genetic interaction results, we next sought to determine whether TDP-43 colocalizes with dFMRP in the Drosophila model and whether any of these puncta were positive for the SG marker PABP. To test this we performed colocalization experiments in primary motor neuron cultures derived from the ventral ganglion of TDP-43 expressing larvae (D42>TDP). We found that TDP-43 was distributed within neurites in puncta that colocalize with dFMRP and PABP (Fig. 2E–O and Supplementary Material, Table S1). Interestingly, while the C-terminus mutation G298S did not have a specific effect on the association between TDP-43 and dFMRP (4% for both TDP^{WT} and TDP^{G298S}, Fig. 2O and Supplementary Material, Table S1), TDP^{G298S} colocalization with PABP was reduced compared to TDP^{WT} (14% for TDP^{WT} compared to 11% for TDP^{G298S}, Fig. 2N, $P_{value} = 0.05$, Supplementary Material, Table S1). Additionally, we measured the colocalization between dFMRP and PABP. In TDP-43 expressing cells, there was significantly more colocalization between dFMRP and PABP compared to cytoplasmic YFP controls (1.5% for cytoplasmic YFP, 6% for both TDP^{WT} and TDP^{G298S}, compare Fig. 2G, H, K, L to C, D arrowheads, see also Fig. 2M and Supplementary Material, Table S1) suggesting that the presence of TDP-43 in neurites leads to increased dFMRP association with PABP positive RNA stress granules. There was no difference in the triple colocalization of TDP-43, dFMRP and PABP between wild-type and the G298S TDP-43 mutant (Supplementary Material, Table S1) consistent with the colocalization data for dFMRP and TDP-43, which was comparable for both TDP-43 variants tested here. These results indicate that a fraction of TDP-43, dFMRP and PABP colocalize in neuronal RNA granules. Given that dFMRP protein and mRNA levels are unaltered by TDP-43 overexpression and dFMRP does not undergo a shift in polysome fractions indicating that it is not a translational target of TDP-43 (Supplementary Material, Fig. S5), our data also show that in the context of cytoplasmic TDP-43, dFMRP is redistributed to RNA stress granules. Colocalization also occurs between TBPH and dFMRP in live cells (Supplementary Material, Fig. S6) indicating that colocalizing puncta observed in neurites are not a result of fixation or human TDP-43 overexpression in Drosophila.

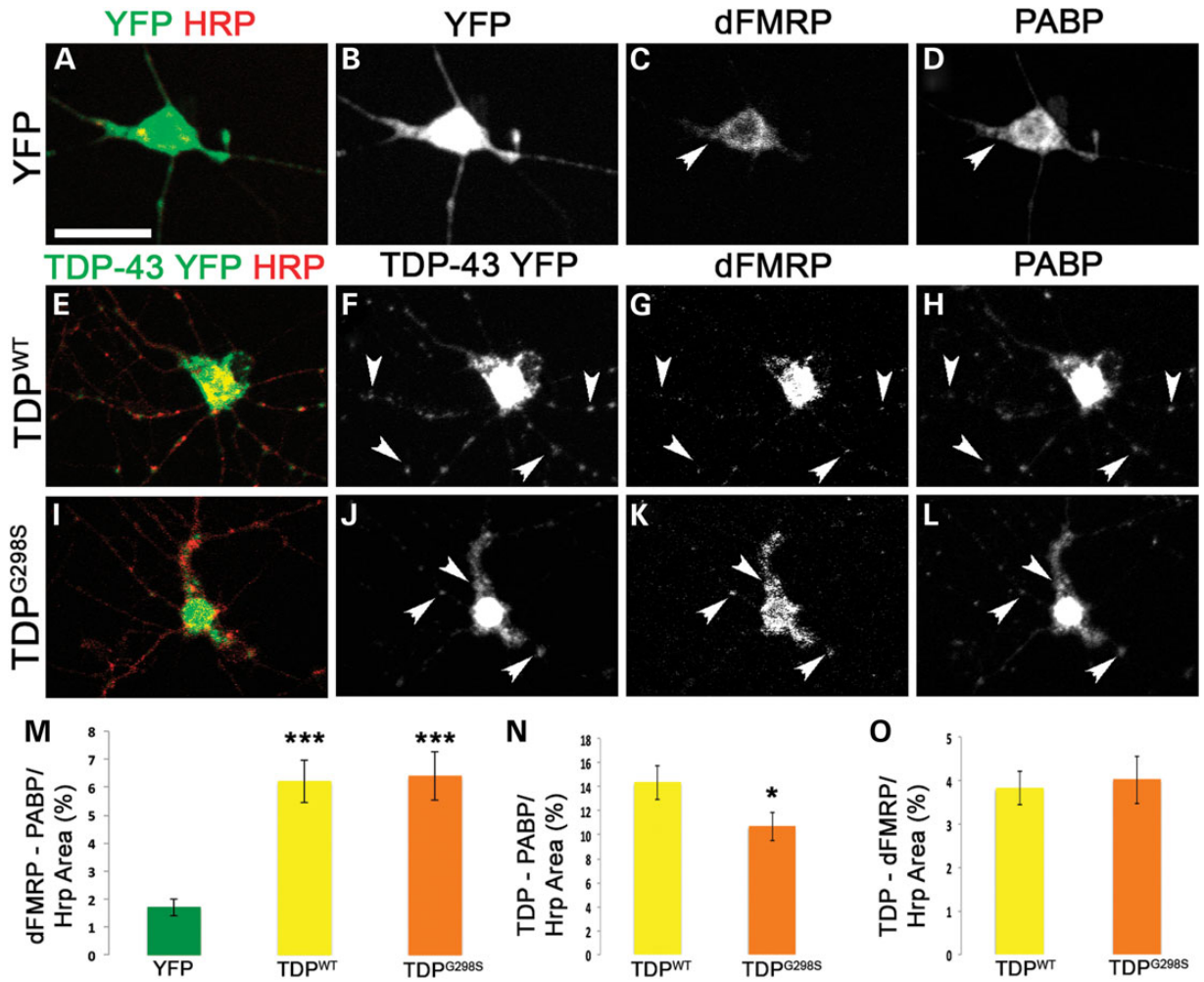

Figure 2. TDP-43, dFMRP and PABP colocalize in neuronal RNA granules in primary motor neurons. (**A–D**) Cytoplasmic YFP expressing cells immunostained with anti-GFP (A and B), anti-dFMRP (C), anti-PABP (D) and anti-Hrp (A) antibodies. (**E–L**) Primary neurons expressing TDP-43 YFP variants (TDP^{WT} E-H, TDP^{G298S} I–L) and immunostained with anti-GFP (E, F, I and J), anti-dFMRP (G and K), anti-PABP (H and L) and anti-HRP (E and I) antibodies. HRP labels neuronal membranes. Genotypes as indicated on the left, immunostains on the top. Arrowheads indicate select colocalizing TDP-dFMRP-PABP granules within neurites. (**M**) Quantification of co-localization between dFMRP and PABP normalized to HRP area. (**N**) Quantification of TDP-43 and PABP co-localization in normalized to HRP area. (**O**) Quantification of co-localization of TDP-43 and dFMRP normalized to HRP area. Student's *T* test was used to calculate *P*-values. $^{*}P < 0.05$. Scale bars: (A) 12 μm.

Additionally, TDP-43 and PABP colocalize in neuronal RNA granules in a TDP-43 variant dependent manner, which suggests that disease associated C-terminal mutations may alter the association with stress granule components such as PABP. Indeed, recent reports have found that C-terminal mutations in TDP-43 alter the dynamics of stress granules formation compared to wild-type TDP-43 (33).

FMRP forms a complex with TDP-43 *in vivo*

Given the genetic interactions and the colocalization data in primary motor neurons, we next tested if TDP-43 forms a complex with dFMRP *in vivo*. Immunoprecipitation experiments from Drosophila heads expressing TDP-43 in the neuroepithelium (with GMR Gal4) showed that endogenous dFMRP associates with TDP-43 (both WT and C-terminal mutant G298S) in a complex (Fig. 3A). Although a small amount of protein can be seen in the IgG lane, FMRP is enriched in the TDP-43 immunoprecipitates compared to controls. Furthermore, binding assays indicate that TDP^{WT} and FMRP can associate *in vitro* with a K_D value of 6.1 nM (4.0–9.4 nM, $n = 4$; Supplementary Material, Fig. S7J). To determine whether the TDP-FMRP complex is conserved in a mammalian model we performed immunoprecipitation experiments from HEK cells expressing wild-type TDP-43 (Fig. 3B) and found that full length TDP-43 (TDP-YFP) associates with endogenous FMRP in a complex (Fig. 3B). Since a mutant lacking the NLS ($TDP^{\Delta NLS}$-YFP) also co-immunoprecipitates with FMRP, our data suggest that this interaction occurs in the cytoplasm (Fig. 3B). Indeed, a TDP-43 variant that does not bind RNA and is restricted to the nucleus (TDP5F-L, 43) does not co-immunoprecipitate with endogenous FMRP (Supplementary Material, Fig. S7H). In keeping with this observation, colocalization experiments in Drosophila primary motor neurons and genetic interactions with TDP^{RRM}, a variant that, like $TDP^{5F\text{-}L}$ does not bind RNA and is restricted to the nucleus ($TDP^{W113A/R151A}$, 28) showed no association or genetic interactions with dFMRP (Supplementary Material, Fig. S7I). These findings indicate that TDP variants associate with FMRP in a complex. Together with the co-localization and co-immunoprecipitation data, these results support a model whereby TDP-43 and FMRP interact directly within neuronal RNA granules.

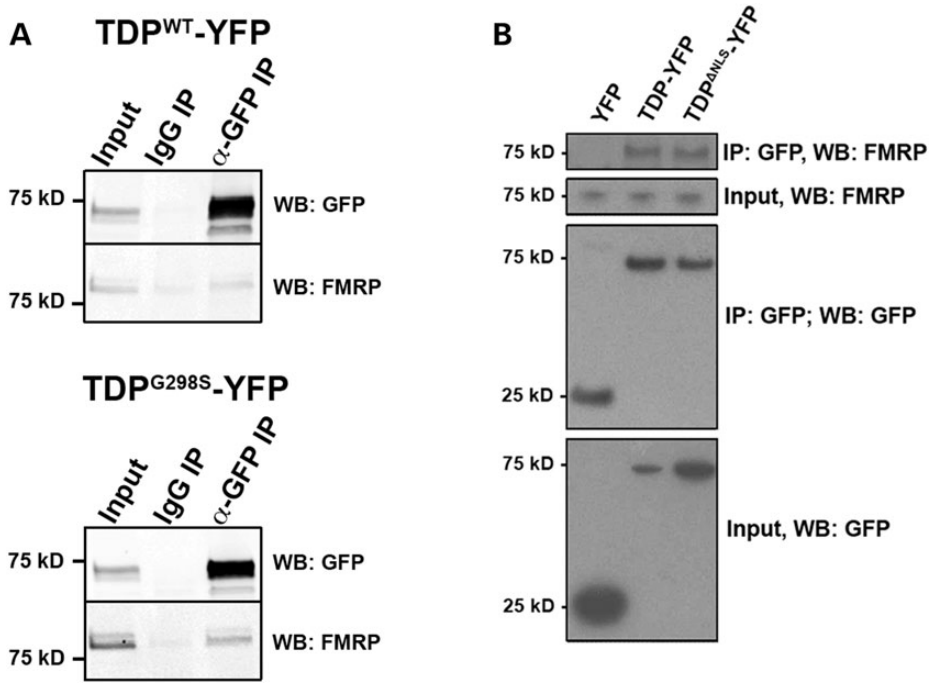

Figure 3. TDP-43 and FMRP form a complex *in vivo*. (**A**) Immunoprecipitation of TDP-43 YFP from Drosophila head extracts. Genotypes as indicated on top. Antibodies used for immunoprecipitation (IP) indicated on top and western blots (WB) indicated on right. (**B**) Immunoprecipitation of TDP-43 YFP variants in HEK cells. Genotypes as indicated on the top. Antibodies used for immunoprecipitation (IP) or western blots (WB) indicated on the right.

dFMRP modulates TDP-43 solubility and molecular mobility

To gain further insights into the molecular mechanism underlying the neuroprotective effects of dFMRP, we next asked whether dFMRP dosage influences the association of TDP-43 with aggregates, which have recently been shown to harbor prion-like properties (44). To test the effect of dFMRP on TDP-43 solubility we performed cellular fractionation experiments using larvae expressing TDP-43 in motor neurons and quantified the amount of TDP-43 present in the soluble, sarkosyl- and urea-soluble/aggregate fractions. dFMRP OE led to a statistically significant decrease in the aggregate (urea) fraction for both wild-type and mutant TDP-43 (Fig. 4A, B, D and E; $P_{value} = 0.014$ and 0.0046, respectively). No notable changes were detected in the solubility of dFMRP alone (Fig. 4C and F). These findings suggest that dFMRP exerts its protective properties by remodeling RNA granules and 'extracting' TDP-43 from aggregates into soluble complexes.

To probe the effect of dFMRP knock-down on TDP-43 we used fluorescence recovery after photobleaching (FRAP) and measured molecular mobility in primary motor neurons derived from larval ventral ganglia. For these experiments, we analyzed individual, non-motile TDP-43-YFP containing RNA granules localized within neurites (see Materials and Methods). In brief, RNA granules were bleached and allowed to recover for 360 s. The recovered fluorescence intensity was recorded every 20 s and plotted against time (Supplementary Material, Fig. S8). As we have previously reported, although the maximum fluorescence recovery was comparable between the two TDP-43 variants analyzed (67% for TDP^{G298S} versus 70% for TDP^{WT}, Supplementary Material, Fig. S8), the kinetics of TDP^{WT} was significantly different from that of TDP^{G298S} (Fig. 4G and Supplementary Material, Fig. S4 and 36). Indeed, the half-life value of TDP^{WT} (i.e. the length of time required for 50% of maximum fluorescence recovery) ranged between 7.7 and 12.6 s while for TDP^{G298S} was 35.7–48.1 s (Supplementary Material, Fig. S8). dFMRP knock-down significantly increased the half-life of TDP-43^{WT} (TDP^{WT} $dFMRP^{RNAi}$), to 31.7–42.8 s (Supplementary Material, Fig. S8), which is comparable to TDP-43^{G298S} alone. Furthermore, reduction of dFMRP levels in the context of TDP-43^{G298S} (TDP^{G298S} $dFMRP^{RNAi}$) also resulted in a significant increase in half-life (49.8–67.2 s) compared to TDP-43^{G298S} alone (Supplementary Material, Fig. S8). Notably, dFMRP knock-down had no significant effect on the half-life of cytoplasmic GFP puncta (Supplementary Material, Fig. S8). These results indicate that a reduction in FMRP levels leads to a specific and significant decrease in the molecular mobility of TDP-43 within neurites. *In vivo*, this may translate into a balance shift towards a more aggregate-like state for TDP-43.

dFMRP OE restores the translation of *futsch* mRNA

The ribostasis hypothesis proposes that the prolonged sequestration of mRNAs and RNA binding proteins by cytoplasmic TDP-43 into SG causes alterations in gene expression that eventually leads to motor neuron disease (38). According to this model, it is possible that dFMRP is trapped in TDP-43 containing complexes or stress granules as indicated by its increased association with PABP in our colocalization experiments, and in turn, this could lead to dysregulation of its own targets. This scenario would predict that known translational targets of dFMRP such as Futsch/MAP1B (45) are upregulated in the context of TDP-43. However, our recent findings that *futsch* mRNA is also a target of TDP-43 in motor neurons (22) and the quantitative western blots shown in Fig. 5D and E indicate that Futsch protein is in fact downregulated at the neuromuscular junction (NMJ) in the context of TDP-43. Furthermore, Futsch expression at the NMJ is restored when dFMRP is overexpressed (Fig. 5D and E). These data suggest an alternate model, whereby dFMRP OE remodels

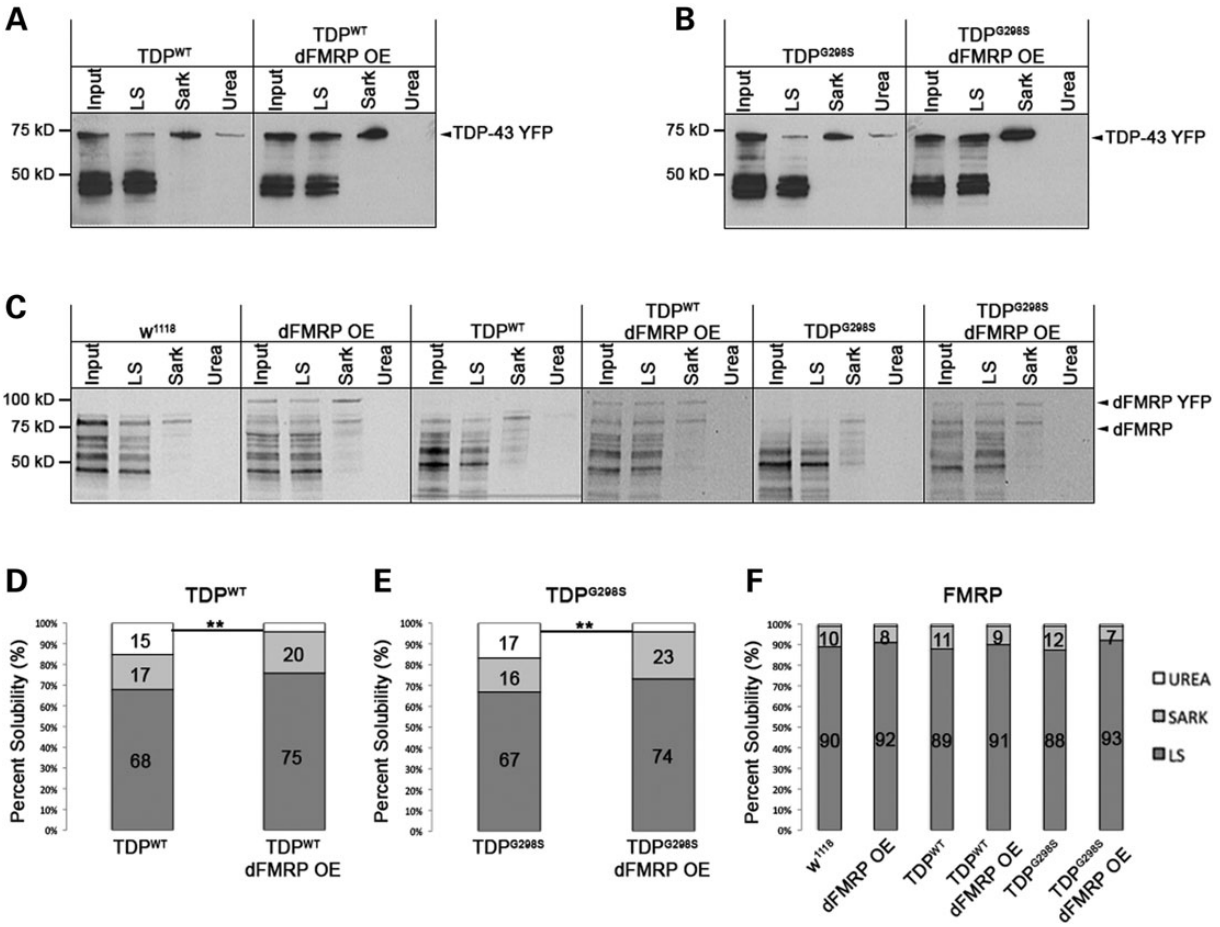

Figure 4. TDP-43 solubility is altered by dFMRP. (**A** and **B**) Solubility studies using third instar larvae show the distribution of TDP-43 variants WT (A) and G298S (B) in low salt (LS), Sarkosyl (Sark) and Urea (U) fractions, alone or in the context of dFMRP overexpression (dFMRP OE). (**C**) The distribution of dFMRP in w^{1118} and dFMRP OE controls in LS, Sark and U fractions and in the context of TDP-43 WT or G298S alone and or with dFMRP OE. (**D–F**) Quantification of WT (D) or G298S (E) TDP-43 and dFMRP (F) levels in LS, Sark, and Urea fractions normalized to input. Statistical significance was determined using Fisher's exact test (**$P < 0.01$).

TDP-43 containing complexes and 'frees' mRNA targets such as *futsch* from sequestration, making them available for translation. This scenario is substantiated by polysome fractionation experiments showing that dFMRP OE indeed restores the shift in the distribution of *futsch* mRNA caused by TDP-43, back from untranslated RNPs to actively translated fractions (Fig. 5F–H). As expected, dFMRP OE alone suppresses *futsch* translation, evidenced by a shift of the transcript from actively translated polysomes to untranslated RNP fractions. Consistent with our findings that TDP-43 and dFMRP associate in a complex and regulate translation, we found that, in the context of TDP-43 expression they co-migrate with actively translating polysome fractions as well as non-actively translating RNP fractions containing monosomes, ribosomal subunits and RNA granules (Fig. 5B and C and Supplementary Material, Table S2). In w^{1118} controls, TBPH, the Drosophila homolog of TDP-43 was also found to be distributed across the RNP and polysome fractions and co-fractionating with dFMRP similar to TDP-43 when overexpressed (Fig. 5A and Supplementary Material, Table S2).

Taken together, our results show that upon dFMRP OE in the context of TDP-43, *futsch* mRNA translation is restored to the levels of w^{1118} controls (Fig. 5D and E). These findings suggest a model whereby dFMRP OE mitigates TDP-43 toxicity by remodeling RNA granules, specifically by extracting TDP-43 and its trapped target mRNAs from RNP complexes to restore translation.

dFMRP OE restores Futsch dependent neuromuscular junction phenotypes

Having previously established Futsch dependent synaptic phenotypes in the context of TDP-43 (22) we turned to the NMJ to further probe the physiological significance of restoring *futsch* mRNA translation via dFMRP OE. Consistent with previous results, using confocal microscopy we found a reduction in Futsch expression at the NMJ in the context of TDP-43 (Fig. 6M) (22). Although as expected, dFMRP OE alone results in reduced Futsch expression at the NMJ (Fig. 6M), co-overexpression of dFMRP and TDP-43 leads to a significant increase in Futsch levels compared to TDP-43 alone (Fig. 6M). This is consistent with our model that dFMRP OE remodels TDP-43 containing RNA granules and restores the translation of *futsch*. Since Futsch has a role in the stabilization of microtubules, we next evaluated the presence of satellite boutons, which correlate with defects in microtubule stability. As we have previously reported, TDP-43 overexpression results in an increase in the number of satellite boutons (Fig. 6C and E arrowheads, Fig. 6N) (14,22). This phenotype is rescued by dFMRP OE (compare Fig. 6I, K to C, E, Fig. 6N) consistent with an

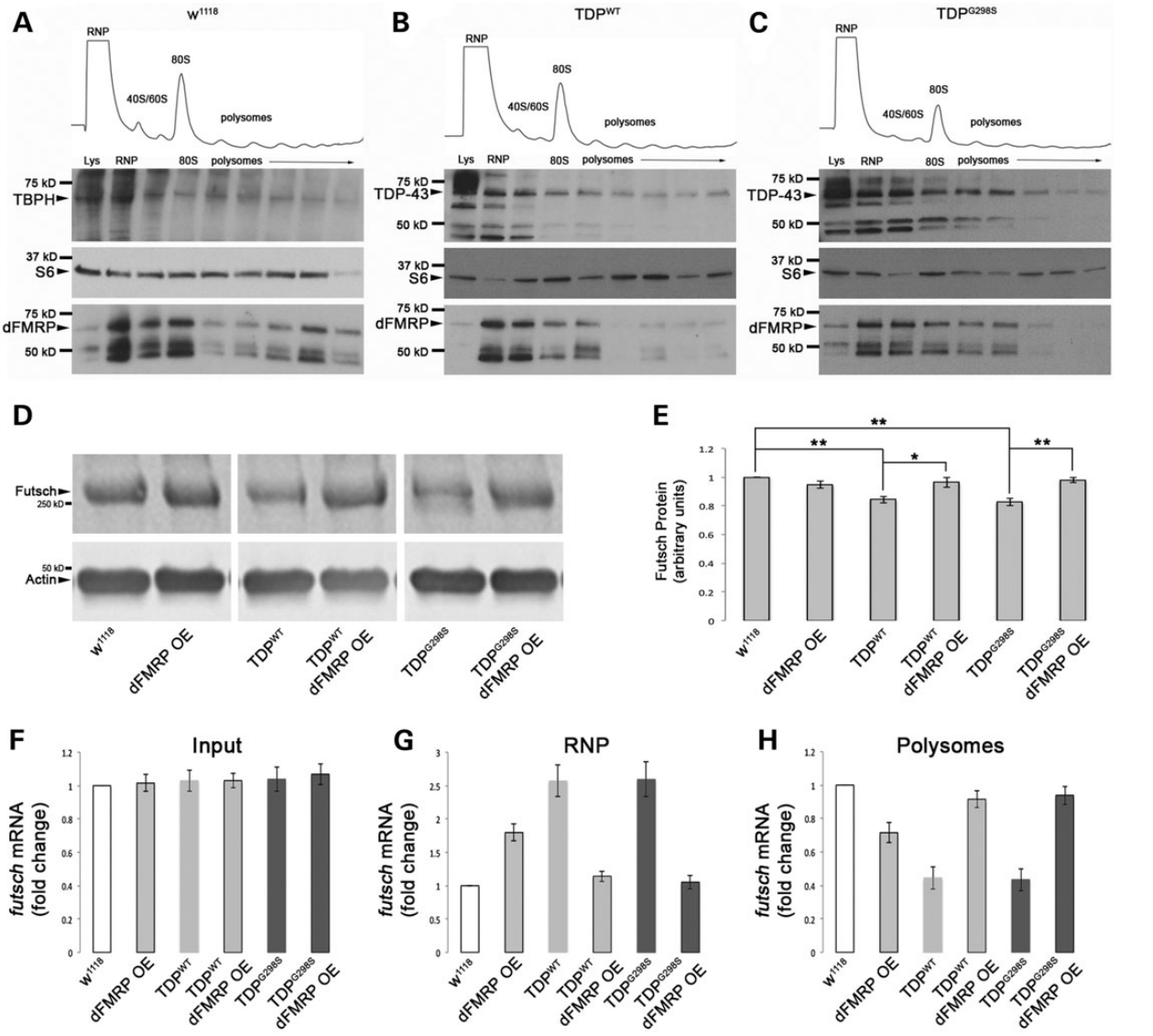

Figure 5. TDP and dFMRP associate with actively translating polysomes to regulate the translation of *futsch*. (**A**) Distribution of TBPH, S6 ribosomal protein, and dFMRP, throughout polysome gradients from w^{1118} controls. (**B** and **C**) Distribution of TDP-43, ribosomal protein S6, and dFMRP throughout polysome gradients in the context of TDP-43 WT (B) or G298S (C). (**D**) Western blot for Futsch protein levels. Antibodies as indicated on left. Actin was used as a loading control. Genotypes as indicated on bottom. (**E**) Quantification of Futsch protein levels normalized to Actin. (**F–H**) qPCR for *futsch* mRNA distribution in polysome fractionation input (F), RNP fractions (G), and polysome fractions (H).

increase in Futsch expression and microtubule stability. Additionally, we examined the presence of Futsch positive loops within synaptic boutons at the NMJ. Futsch loops are associated with stable synaptic contacts and correlate with areas of microtubule stability. Upon expression of TDP-43 (WT or G298S) we find a significant reduction in the number of Futsch loops compared to controls (compare Fig. 6D, F to B, Fig. 6O). When dFMRP is co-overexpressed with TDP-43 this phenotype is also rescued (Fig. 6J, L and O) indicating that restoration of Futsch expression at the NMJ via dFMRP OE mitigates several TDP-43 mediated structural abnormalities at the neuromuscular synapse.

Discussion

Here we used a combination of genetic and molecular approaches to uncover a novel functional interaction between dFMRP and TDP-43. Taken together, our results support a model whereby dFMRP, a well-established translational regulator, can modulate the neurotoxicity caused by TDP-43 overexpression. When overexpressed, dFMRP decreases the association of TDP-43 with the aggregate-like fraction. Together with our immunoprecipitation and binding experiments, these findings support a model whereby dFMRP promotes the remodeling of the RNP by 'extracting' TDP-43 and freeing the sequestered mRNA from the protein-RNA complex. This in turn may alleviate the negative impact that TDP-43 exerts on its mRNA targets as is the case for *futsch* mRNA (see Fig. 7 for model). Indeed, dFMRP OE in the context of TDP-43 restores the expression of *futsch*, which is a translation target of TDP-43 (22). While the change in Futsch expression is slight in magnitude, it is statistically significant. These findings suggest a scenario whereby the robust synaptic phenotypes observed in ALS may result from the combinatorial effect of decreased expression for multiple TDP-43 targets at the NMJ. In future studies it will be interesting to determine additional

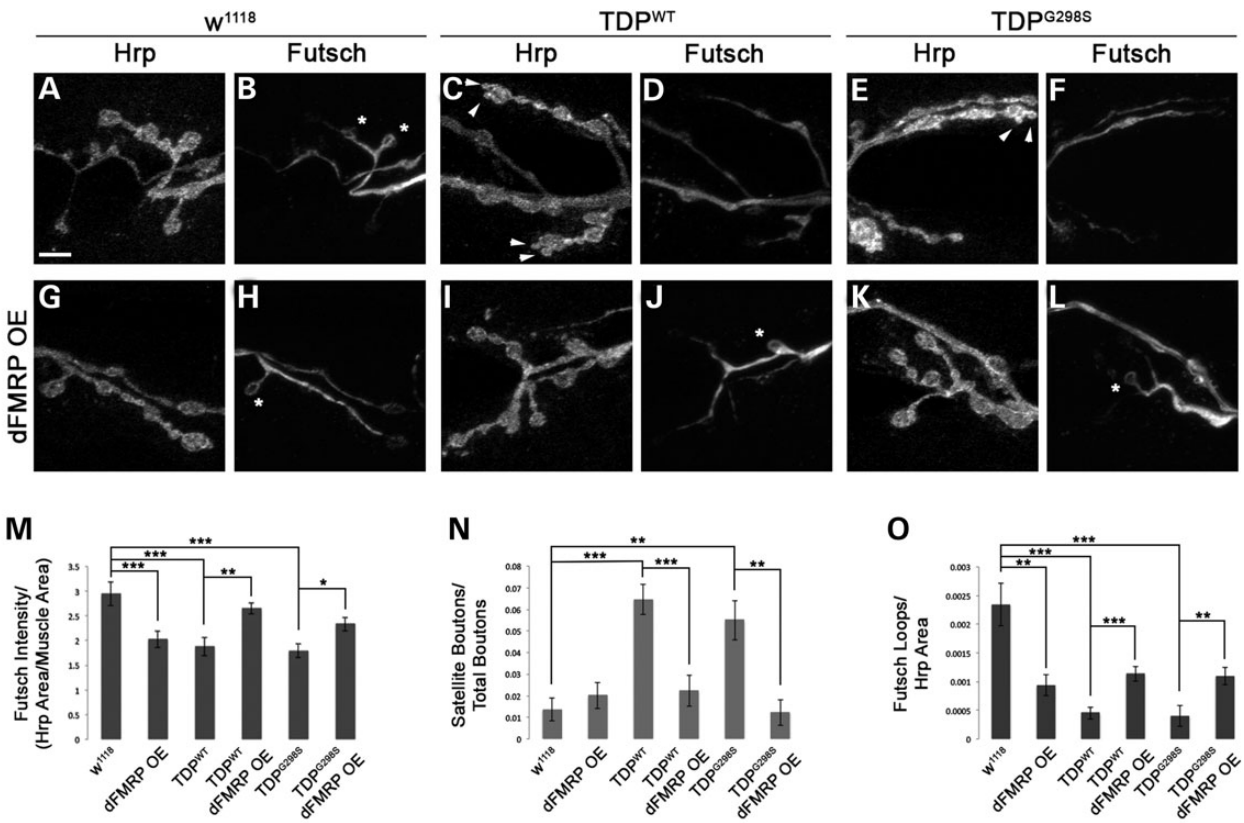

Figure 6. Futsch dependent neuromuscular junction alterations are restored by dFMRP OE. (**A–F**) Larval neuromuscular junctions of D42>w^{1118} controls (A and B) and larvae expressing TDP-43^{WT} (C and D) or TDP-43^{G298S} (E and F) in motor neurons, immunostained for the neuronal membrane marker HRP (A, C and E) and Futsch (B, D and F). Arrow heads indicate satellite boutons. Asterisks indicate Futsch loops. (**G–L**) Larval neuromuscular junctions of dFMRP OE in a TDP-43^{WT} (I and J) or TDP-43^{G298S} (K and L) background compared to dFMRP OE controls (G and H), immunostained the neuronal membrane marker HRP (G, I and K) and Futsch (H, J and L). Arrowheads indicate satellite boutons. Asterisks indicate Futsch loops. (**M–O**) Quantification of Futsch Intensity (M), satellite boutons (N), and Futsch loops (O). Scale bar (A) 5 μm.

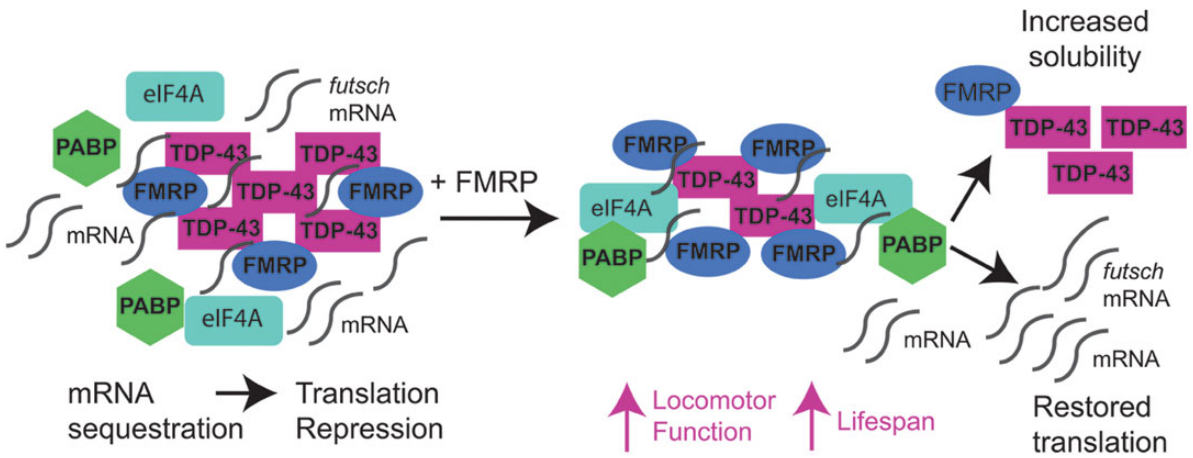

Figure 7. A model for TDP-43–dFMRP interaction. dFMRP OE is neuroprotective and modulates TDP-43 solubility as demonstrated by fractionations and FRAP experiments. dFMRP OE in the context of TDP-43 OE restores translation of specific mRNA targets as demonstrated by polysome experiments.

synaptic targets of TDP-43 whose expression is restored upon dFMRP OE. While *futsch* mRNA can be translationally controlled by both dFMRP and TDP-43, in the context of TDP-43 RNA granules, dFMRP appears to favor an association with TDP-43 protein over its translation target, leaving *futsch* mRNA available for protein synthesis, which explains the translation restoration we observed in the context of dFMRP OE. Given the wide repertoire of RNA binding protein partners of TDP-43 (28), it will be interesting in the future to determine whether others can also confer neuroprotection to TDP-43-dependent toxicity and whether they do so by a similar molecular mechanism. This would be expected given that Futsch expression is significantly increased but not fully restored by dFMRP OE at the NMJ (Fig. 6M).

We have previously shown that TDP^{WT} and disease linked mutations, although expressed at comparable levels, confer differential toxicity in various phenotypic assays (14,36). Here we provide evidence that TDP^{WT} and TDP^{G298S} also interact differentially with protein partners. TDP^{G298S} colocalizes with PABP to a lesser extent than TDP^{WT}. We also provide further evidence that TDP^{WT} and TDP^{G298S} exhibit distinct molecular mobilities within neurites, which is consistent with previous reports that although wild-type and disease linked variants both associate with stress granules, their dynamics, persistence and size differ dramatically (33). Taken together, our findings and these published data suggest that ALS may be a consequence of chronic translation inhibition (Fig. 7). This could result from dysregulation of RNA granule physiology in the context of excess cellular stress as previously suggested (38–40). This scenario is consistent with previous findings that inhibition of SG is neuroprotective (46) and provides a plausible mechanism for how TDP-43 mutations lead to disease. Additionally, it can explain the association of wild-type TDP-43 with cytoplasmic aggregates in the majority of ALS cases, regardless of etiology. One possibility is that, in the context of aging related or other cellular stress, wild-type TDP-43 enters the RNA stress granule cycle, contributing to translation inhibition and disease pathophysiology.

Our results indicate that FMRP remodels TDP-43 RNP granules and this restores *futsch* translation and expression at the NMJ. This in turn, can alleviate phenotypes associated with microtubule instability such as the presence of satellite boutons. Altered microtubule stability is emerging as a prominent pathological mechanism underlying the progression of ALS (22,47) and may provide a useful avenue for the development of therapeutics. In addition, altered ribostasis has emerged as a major hypothesis for explaining the progression from RNA stress granules to aggregates seen in disease. This model suggests altered translational regulation as a molecular mechanism underlying disease progression. Our results support this model and provide evidence that mitigating translational repression can suppress disease phenotypes. In future studies it will be important to establish whether blanket approaches such as RNA SG inhibition or translation restoration offer more promise than targeted strategies based on specific targets.

Two recent studies have shown that TDP-43 suppresses toxicity in CGG repeat expansion models of Fragile X associated tremor/ataxia syndrome (FXTAS) (48,49). Removing a portion of the C-terminus of TDP-43 in which interactions with hnRNP A2/B1 typically occur, abolishes the ability of TDP-43 to suppress toxicity (48). These results suggest that TDP-43 may work to mitigate CGG RNA toxicity via interactions with its protein partners by preventing them from sequestration into toxic RNA foci. Thus, in the case of CGG repeat disorders, TDP-43 may alter RNP complexes similar to how dFMRP OE alters RNP complexes in our TDP-43 model of ALS. Together with these studies, our results provide evidence for common mechanisms underlying neurodegenerative diseases and repeat expansion disorders. In both cases, remodeling of RNP granules and the 'freeing' of RNA binding proteins or mRNA targets mitigates toxicity.

In conclusion, we identify a novel strategy for mitigating TDP-43-dependent phenotypes *in vivo*, based on FMRP mediated remodeling of RNA granules, which provides relief to chronic translation inhibition for specific mRNA targets such as *futsch*. Our results suggest that targeting RNP remodeling or translation restoration may prove useful as therapeutic strategies. Future experiments are aimed at identifying additional translational targets of TDP-43 *in vivo* that will broaden the repertoire of therapeutic strategies for ALS and related neurodegenerative diseases.

Materials and Methods

Drosophila genetics

All Drosophila stocks and crosses were kept on standard yeast/cornmeal/molasses food at 25°C unless otherwise noted. Human TDP-43 variants with YFP C-terminal tags and Drosophila TBPH variants with RFP C-terminal tags were generated as previously described (14,36). Gal4 drivers used included the eye-specific GMR Gal4 and the motor neuron driver D42 Gal4 (50). For controls, w^{1118} was crossed with the appropriate Gal4 driver. To manipulate dFMRP we used $dFMRP^{RNAi}$ (w^{1118}; P{GD1288}v8933; Vienna Drosophila RNAi Center) or UAS-YFP dFMRP (42). w^{1118}; P{GD6943}v38377 and w^{1118}; P{GD6943}v38379 (Vienna Drosophila RNAi Center) were used to knock down TBPH. To test for Gal4 dilution effect we used UAS-mCD8-ChRFP (Bloomington Stock Center).

Adult eye imaging

15-day-old adult female fly eyes were imaged with a Leica MZ6 microscope equipped with an Olympus DP73 camera and controlled by Olympus DP Controller and Olympus DP Manager software. Individual images were processed with Adobe Photoshop CS6 (Adobe) as previously described (14,36).

Larval turning assays

Assays were performed as previously described (14). Briefly, crosses were made at 22°C and wandering third instar larvae were placed on a grape juice plate. After a 30 s acclimation period, crawling larvae were gently turned on their back (ventral side up). They were observed until they were able to turn over (dorsal side up) and make a forward motion. The time it took to complete this task was recorded for ≥30 larvae per genotype. A student's *t*-test was performed to determine statistical significance.

Lifespan analysis

All crosses were carried out at 22°C. Newly eclosed males were placed in a new vial every 7 days. Survival plots were generated using the survival and Hmisc packages in R and RStudio software. Statistical analysis was done using the log-rank test in R.

Immunohistochemistry and confocal imaging

Larval motor neurons were prepared as previously described (36) followed by fixation in 3.5% formaldehyde in PBS, pH 7.2 for 20 min then permeabilized with 0.3% Triton X-100. Blocking agent consisted on 2% BSA and 5% normal goat serum. The following antibodies were used: mouse anti-dFMRP 6A15 at 1:300 (Abcam), rabbit anti-PABP at 1:1500 (from Matthias Henze), anti-GFP-FITC at 1:300 (Rockland), anti-HRP Cy5 at 1:50 (Jackson), anti-rabbit Alexa 405 at 1:400 (Molecular Probes), anti-mouse Alexa 568 at 1:500 (Molecular Probes). For TDP^{RRM} expressing cells the following antibodies were used: rabbit anti-TDP-43 at 1:500 (Protein Tech), mouse anti-dFMRP 6A15 at 1:300, anti-rabbit FITC at 1:300 (Molecular Probes), anti-mouse Cy5 at 1:300 (Jackson), and anti-HRP TRITC at 1:50 (Jackson). Cells were imaged using a Zeiss Meta LSM 510 confocal microscope. The split channels tool in NIH image J was used to separate dFMRP, PABP, and GFP (TDP-43) into single channel images. The Colocalization Threshold Tool Plugin was then used to obtain an image of colocalized pixels between the TDP-43 and PABP channels. All channels (TDP-43, dFMRP, PABP, HRP, TDP-43—PABP colocalized)

were thresholded in MetaMorph to eliminate single pixel background noise. Using the HRP image, a ROI was drawn in MetaMorph to exclude the cell body. This ROI was applied to all subsequent channels or colocalized channels. MetaMorph software was used to calculate the total pixel areas of PABP, dFMRP, TDP-43, TDP-43/PABP, and HRP within individual neurons from single channel or overlapped pixel images obtained with NIH Image J. The percentage of dFMRP and TDP, PABP and TDP-43, or TDP-43/PABP and dFMRP pixel overlap was normalized to total HRP area and represents overlap specifically in neurites.

For live cell imaging experiments, larval motor neurons from larvae expressing dFMRP YFP and $TBPH^{WT}$ RFP were prepared as described above. Cells were imaged in 1× PBS as described above.

Larval NMJs were prepared as previously described (14,22,36). Briefly, wandering third instar larvae were filleted in HL-3 saline, pinned out on Sylgard dishes and fixed in 3.5% formaldehyde in PBS, pH 7.2 for 30 min, then permeabilized with 0.1% Triton X-100. Blocking agent consisted of 2% BSA and 5% normal goat serum. The following antibodies were used: anti-Futsch at 1:50 (mAb 22C10, DSHB), anti-mouse Alexa 568 at 1:500 (Molecular Probes), and anti-HRP-Cy5 at 1:200 (Molecular Probes). Phalloidin-488 (Molecular Probes) was used at 1:400 to visualize muscles. Larval muscles 6–7, segment A3 were imaged using a Zeiss LSM 510 confocal microscope. NIH Image J was used to quantify Futsch intensity as well as to count bouton and satellite bouton numbers and Futsch loops. Measurements were normalized to HRP and muscle areas to account for size variations (22,36).

Cellular fractionations and western blotting

25 wandering third-instar larvae were homogenized in 250 μL low-salt buffer (LS) (10 mM Tris, 5 mM EDTA, 10% sucrose, pH 7.5). Homogenates were briefly centrifuged at 2000*g* for 30 s. Fat and cuticle were discarded and 50 μl homogenate was set aside as input. The remaining 200 μl homogenate was centrifuged at 25 000*g* for 30 min. The supernatant from this step represents the LS fraction. The pellet was further extracted with ionic detergent containing buffer (Sark) (10 mM Tris, 5 mM EDTA, 1% sarkosyl, 10% sucrose, pH 7.5) and 180 000*g* for 20 min. The supernatant from this step represents the Sark fraction. The remaining detergent insoluble pellet was solubilized in urea containing buffer (Urea) (30 mM Tris, 7 M urea, 2 M thiourea, 4% CHAPS, pH 8.5). All buffers contained Complete protease inhibitor cocktail (Roche) supplemented with 0.5 mM phenylmethylsulfonyl fluoride to block proteolysis. Protein concentrations were calculated using Qubit (Invitrogen) and 25 μg of protein was loaded for each sample. Equal volume of 2× Laemmli buffer was added to individual fractions, which were resolved on 4–20% SDS-PAGE precast gradient gels (BioRad) and then transferred to a nitrocellulose membrane (BioRad) for western blotting. The following primary antibodies were used: rabbit anti-GFP at 1:6000 (Invitrogen), and mouse anti-Drosophila FMRP 6A15 at 1:2000 (Abcam). The secondary antibody was goat anti-rabbit-conjugated-HRP at 1:1000 (Thermo Scientific) or 1: 10 000 goat anti-mouse IRDye 800 (Licor). Proteins were detected using SuperSignal West Femto Substrate (Thermo Scientific) or the Licor Odyssey system, and bands spanning the entire lane were quantified using NIH Image J software. TDP-43 or dFMRP levels in individual fractions were normalized to input. Fisher's exact test was used to determine statistical significance.

Western blots for Futsch: Drosophila NMJs were prepared by filleting wandering third instar larvae in HL-3 saline. Axons were cut just below the ventral nerve cord and retained with the NMJ preparation. The ventral nerve cord was discarded. Preparations were homogenized in 2× Laemmli buffer. Samples were resolved on 4–20% SDS-PAGE gradient gels (BioRad) and transferred overnight on to a nitrocellulose membrane (BioRad). The following primary antibodies were used: 1:3000 mouse anti-22C10 (DSHB), and 1:15 000 rabbit anti-β Actin (Cell Signaling). Secondary antibodies used were: 1:10 000 goat anti-rabbit IRDye 800 (Licor) and 1:10 000 goat anti-mouse IRDye 800 (Licor). Detection was conducted with the Licor Odyssey system and quantification performed as described above.

Western blots for TDP-43 and dFMRP: Third instar wandering larvae were flash frozen in liquid nitrogen and homogenized in 2× Laemmli buffer and resolved as above. Western blots were conducted as above. The following primary antibodies were used: 1:6000 rabbit anti-GFP (Life Technologies) and 1:2000 mouse anti-dFMRP 6A15 (Abcam). Secondary antibodies, detection method, and quantification as described above.

Fluorescence recovery after photobleaching

Larval motor neurons were isolated from third instar wandering larvae expressing TDP-43 tagged with YFP as previously described (36). FRAP was performed and analyzed as previously described (51).

Immunoprecipitation experiments

Heads from $GMR>TDP^{WT}$ or $GMR>TDP^{G298S}$ flies were collected, frozen, ground into fine powder then resuspended in 1.5 ml of Lysis buffer (50 mM HEPES pH 7.4, 0.5% Triton X-100, 150 mM NaCl, 30 mM EDTA, 7× Protease Inhibitor Cocktail (Roche), 40 U/μl RNasin Plus (Promega), 0.2 mM phenylmethanesulfonyl fluoride (PMSF). Following homogenization the cell lysate was cleared of debris by centrifugation at 7000 rpm for 10 min at 4°C. 10 μg of Rabbit anti-GFP polyclonal antibody (Life Technologies) was added to the lysate and incubated for 2 h at 4°C. Next, Dynabeads Protein A were added and incubated for 2 h at 4°C. 10 μg of Rabbit IgG (Roche) was used a control. The Dynabeads Protein A immune complexes were washed three times for 5 min each in wash buffer (50 mM HEPES pH 7.4, 0.5% Triton X-100, 100 mM NaCl, 30 mM EDTA). The immune complexes were collected, resuspended in 1× Laemmli buffer (0.0625 M Tris HCl, 2% SDS, 10% glycerol, 0.002% bromophenol blue) and analyzed by immunoblotting using standard procedures. Chicken anti-GFP at 1:15 000 (Abcam) and Mouse anti-dFMRP at 1:2000 (Abcam) were used to probe TDP-43 and FMRP, respectively.

Immunoprecipitations from mammalian cells: co-immunoprecipitations in mammalian cells were performed from HEK293T cells transfected with TDP-43–YFP fusion constructs using FuGene 6 (Roche) according to the manufacturer's instructions. After 48 h, cells were washed with PBS, trypsinized and collected by centrifugation. Cells were washed in ice-cold PBS containing protease inhibitor cocktail (Roche) then lysed in NP-40 lysis buffer (150 mM NaCl, 50 mM Tris, pH 8.0, 1% NP-40 and protease inhibitors). Lysates were clarified by centrifugation and pre-cleared with protein A agarose (Invitrogen). Immunoprecipitation was performed by incubating with anti-GFP rabbit polyclonal antibody (1:750 dilution; Abcam) for 2 h, then protein A agarose beads (50 μl) for 1 h. The beads were washed three times with NP-40 lysis buffer and resuspended in 4× SDS sample buffer (40% glycerol, 240 mM Tris HCL pH 6.8, 8% SDS, 0.04% bromophenol blue, 5% b-mercaptoethanol). Lysates were boiled for 5 min, then subjected to SDS–PAGE (4–12% gradient Bis-Tris, Invitrogen) and transferred to PVDF membrane (Invitrogen). Membranes were blocked for 1 h in 5% non-fat dry milk at room

temperature and then incubated O/N in primary antibody at 4°C. Membranes were washed four times in PBS, then incubated in HRP-conjugated secondary antibody (1:5000) for 1 h, then washed four times in PBST (PBS + 0.1% Tween20). Proteins were detected with Immobilon Western Chemiluminescent HRP Substrate (Millipore) and visualized on Biomax MR film (Kodak). Primary antibodies were: anti-GFP mouse polyclonal antibody (Roche) at 1/1000 and anti-FMRP mouse antibody (Abcam) at 1:1000.

In vitro binding assays

Human FMRP (isoform 7) in a pET 21a expression vector containing an N-terminal 6XHIS tag (kindly provided by Dr Stephanie Ceman, UIUC) was transformed into *Escherichia Coli* (BL23-DE3). Expression was induced with 0.3 mM IPTG 12–16 h at room temperature. Soluble proteins were extracted from the bacterial pellet and HIS-FRMP was purified (~70%) using Ni-NTA agarose (EMD Millipore) according to standard protocols. Purified N-terminal GST-tagged full length TDP-43 was obtained from ProteinTech Group.

Interactions between GST-TDP-43 and HIS-FMRP were characterized using homogenous time-resolved fluorescence (HTRF) technology as previously described (52,53). Anti-HIS and anti-GST mouse monoclonal antibodies conjugated to HTRF donors and acceptors were purchased from Cis-Bio Inc: anti-GST terbium (Tb) HTRF donor, anti-HIS d2 HTRF acceptor. Various concentrations of both TDP-43 and FRMP was incubated for 2 h at room temperature in 10 µl of assay buffer (20 mM Tris, pH 7.0, 2 mM $MgCl_2$, 0.3 mM EGTA, 0.1% CHAPS) in either the absence and presence of oligonucleotides. After incubation, 5 µl of anti-GST and anti-HIS HTRF donor and acceptor molecules were added to each well at the manufacturers suggested concentrations followed by 1 h incubation at room temperature. Time-resolved fluorescence measurements were obtained using a Synergy 2 plate reader (Biotek, Winooski, VT, USA) using excitation wavelength of 330 nm and emission wavelengths of 620 nm and 665 nm, with a 250 µsec delay between excitation and emission. Data were shown as a ratio of $RFU_{665}/RFU_{620} \times 1000$.

Polysome fractionations

150 mg of adult frozen flies were ground and homogenized in 1 ml buffer containing 25 mM Tris–HCl pH 7.5, 250 mM NaCl, 250 mM NH_4Cl, 50 mM $MgCl_2$, 250 mM sucrose, 1 mg/ml cycloheximide, 100 U/ml RNasin, 1% Triton, and 0.5% β-mercaptoethanol. Polysomes were separated by centrifugation on 15–50% sucrose gradients at ~200 000*g* for 3 h, then fractionated using a flow-through spectrophotometer (Brandel) at 254 nm. RNA was precipitated from fractions using Trizol (Life Technologies). Protein was precipitated using TCA and acetone, after which the pellet was dissolved in 50 µl of 0.5 M Tris, pH 11 and 3% SDS. 25 µg of protein was loaded in each lane, subjected to SDS-PAGE and western blotting as described for cellular fractionation experiments. TBPH was detected using rabbit anti-TBPH at 1:3000 (from Dr Fabian Feiguin). S6 ribosomal protein was detected using mAb #2317 (Cell Signaling) at 1:500. All other antibodies, detection methods, and quantification as described above.

qRT-PCR

Polysome fractionations: following polysome fractionation, fractions corresponding to the RNP, 40/60S, and 80S peaks were pooled for RNA isolation from the 'RNP' or untranslated fraction. RNA from 2+ polysomes was pooled as the 'polysome' or actively translating fraction. RNA precipitation was carried out with Trizol (Life Technologies). First strand cDNA synthesis was performed with a Superscript III cDNA synthesis kit (Invitrogen). qPCR reactions were conducted with SYBR select master mix (Applied Biosystems) and an ABI 7300 Real Time PCR System (Applied Biosystems). Primers were used as follows: Futsch 6/7 exon-exon junction (F: TAACATGCTTGTTGACGGCG and R: CCCTTGCGGTCAGGTACATT), and GAPDH (F: CCGCAGTGCTT GTTTTGCT and R: TATGGCCGAACCCCAGTTG). Samples were prepared and run in triplicate. Fractions were normalized to their respective inputs and fold changes were then calculated compared to w^{1118} using standard ΔΔCT methods (54).

qPCR from whole larvae: Total RNA was prepared from wandering third instar larvae using an RNeasy Kit (Qiagen) with on-column DNAse treatment. First strand cDNA synthesis was performed with a Superscript III cDNA synthesis Kit (Invitrogen). qPCR reactions were conducted with SYBR Select Master Mix (Applied Biosystems) and an ABI 7300 Real Time PCR System (Applied Biosystems). The following primers were used: GAPDH (F: CCGCAGTGCTTGTTTTGCT and R: TATGGCCGAACCCCAGTTG), TDP-43 (F: ACAACCGAACAGGACCTG and R: GGCTCATCTTGGC TTTGC), and dFMRP (F: CGATTGTAAACGGGTGGC and R: CAAA TGTTGCTGCTGGCCG).

Supplementary Material

Supplementary Material is available at *HMG* online.

Acknowledgements

We thank Stephanie Ceman (UIUC) for providing the human FMRP plasmid, Mathias Hentze (EMBL) for the PABP antibody, Fabian Feiguin (ICGEB, Trieste) for the TBPH antibody, and Bob Kraft for comments on the manuscript. The 22C10 monoclonal antibody developed by S. Benzer was obtained from the Developmental Studies Hybridoma Bank developed under the auspices of the NICHD and maintained by The University of Iowa, Department of Biology, Iowa City, IA 52242.

Conflict of Interest statement. None declared.

Funding

This work was funded by National Institues of Health NS078429 and Muscular Dystrophy Association 255293 grants (to D.C.Z.), National Institues of Health NS073660, NS065317 (to A.D.G.), Target ALS, Packard Foundation and ALSAC (to J.P.T.), National Institues of Health NS072749 (to A.B.R.). Additional funds were provided by the Himelic Family Foundation, the Neuroscience Graduate Interdisciplinary Program at UA (to A.N.C.).

References

1. Banks, G.T., Kuta, A., Isaacs, A.M. and Fisher, E.M. (2008) TDP-43 is a culprit in human neurodegeneration, and not just an innocent bystander. *Mamm. Genome*, **19**, 299–305.
2. Gendron, T.F., Cosio, D.M. and Petrucelli, L. (2013) c9RAN translation: a potential therapeutic target for the treatment of amyotrophic lateral sclerosis and frontotemporal dementia. *Expert Opin. Ther. Targets*, **17**, 991–995.
3. Robberecht, W. and Philips, T. (2013) The changing scene of amyotrophic lateral sclerosis. *Nat. Rev. Neurosci.*, **14**, 248–264.
4. Lagier-Tourenne, C. and Cleveland, D.W. (2009) Rethinking ALS: the FUS about TDP-43. *Cell*, **136**, 1001–1004.

5. Ling, S.C., Polymenidou, M. and Cleveland, D.W. (2013) Converging mechanisms in ALS and FTD: disrupted RNA and protein homeostasis. *Neuron*, **79**, 416–438.
6. Neumann, M., Sampathu, D.M., Kwong, L.K., Truax, A.C., Micsenyi, M.C., Chou, T.T., Bruce, J., Schuck, T., Grossman, M., Clark, C.M. *et al.* (2006) Ubiquitinated TDP-43 in frontotemporal lobar degeneration and amyotrophic lateral sclerosis. *Science*, **314**, 130–133.
7. Sreedharan, J., Blair, I.P., Tripathi, V.B., Hu, X., Vance, C., Rogelj, B., Ackerley, S., Durnall, J.C., Williams, K.L., Buratti, E. *et al.* (2008) TDP-43 mutations in familial and sporadic amyotrophic lateral sclerosis. *Science*, **319**, 1668–1672.
8. Van Deerlin, V.M., Leverenz, J.B., Bekris, L.M., Bird, T.D., Yuan, W., Elman, L.B., Clay, D., Wood, E.M., Chen-Plotkin, A.S., Martinez-Lage, M. *et al.* (2008) TARDBP mutations in amyotrophic lateral sclerosis with TDP-43 neuropathology: a genetic and histopathological analysis. *Lancet Neurol.*, **7**, 409–416.
9. Kabashi, E., Valdmanis, P.N., Dion, P., Spiegelman, D., McConkey, B.J., Vande Velde, C., Bouchard, J.P., Lacomblez, L., Pochigaeva, K., Salachas, F. *et al.* (2008) TARDBP mutations in individuals with sporadic and familial amyotrophic lateral sclerosis. *Nat. Genet.*, **40**, 572–574.
10. Janssens, J. and Van Broeckhoven, C. (2013) Pathological mechanisms underlying TDP-43 driven neurodegeneration in FTLD-ALS spectrum disorders. *Hum. Mol. Genet.*, **22**, R77–R87.
11. Johnson, B.S., Snead, D., Lee, J.J., McCaffery, J.M., Shorter, J. and Gitler, A.D. (2009) TDP-43 is intrinsically aggregation-prone and ALS-linked mutations accelerate aggregation and increase toxicity. *J. Biol. Chem.*, **284**, 20329–20339.
12. Da Cruz, S. and Cleveland, D.W. (2011) Understanding the role of TDP-43 and FUS/TLS in ALS and beyond. *Curr. Opin. Neurobiol.*, **21**, 904–919.
13. Couthouis, J., Hart, M.P., Shorter, J., DeJesus-Hernandez, M., Erion, R., Oristano, R., Liu, A.X., Ramos, D., Jethava, N., Hosangadi, D. *et al.* (2011) A yeast functional screen predicts new candidate ALS disease genes. *Proc. Natl. Acad. Sci. USA*, **108**, 20881–20890.
14. Estes, P.S., Boehringer, A., Zwick, R., Tang, J.E., Grigsby, B. and Zarnescu, D.C. (2011) Wild-type and A315T mutant TDP-43 exert differential neurotoxicity in a Drosophila model of ALS. *Hum. Mol. Genet.*, **20**, 2308–2321.
15. Kabashi, E., Bercier, V., Lissouba, A., Liao, M., Brustein, E., Rouleau, G.A. and Drapeau, P. (2011) FUS and TARDBP but not SOD1 interact in genetic models of amyotrophic lateral sclerosis. *PLoS Genet.*, **7**, e1002214.
16. Laird, A.S., Van Hoecke, A., De Muynck, L., Timmers, M., Van den Bosch, L., Van Damme, P. and Robberecht, W. (2010) Progranulin is neurotrophic in vivo and protects against a mutant TDP-43 induced axonopathy. *PLoS ONE*, **5**, e13368.
17. Li, Y., Ray, P., Rao, E.J., Shi, C., Guo, W., Chen, X., Woodruff, E.A. III, Fushimi, K. and Wu, J.Y. (2010) A Drosophila model for TDP-43 proteinopathy. *Proc. Natl. Acad. Sci. USA*, **107**, 3169–3174.
18. Liachko, N.F., Guthrie, C.R. and Kraemer, B.C. (2010) Phosphorylation promotes neurotoxicity in a *Caenorhabditis elegans* model of TDP-43 proteinopathy. *J. Neurosci.*, **30**, 16208–16219.
19. Lu, Y., Ferris, J. and Gao, F.B. (2009) Frontotemporal dementia and amyotrophic lateral sclerosis-associated disease protein TDP-43 promotes dendritic branching. *Mol. Brain*, **2**, 30.
20. Wegorzewska, I., Bell, S., Cairns, N.J., Miller, T.M. and Baloh, R.H. (2009) TDP-43 mutant transgenic mice develop features of ALS and frontotemporal lobar degeneration. *Proc. Natl. Acad. Sci. USA*, **106**, 18809–18814.
21. Alami, N.H., Smith, R.B., Carrasco, M.A., Williams, L.A., Winborn, C.S., Han, S.S., Kiskinis, E., Winborn, B., Freibaum, B.D., Kanagaraj, A. *et al.* (2014) Axonal transport of TDP-43 mRNA granules is impaired by ALS-causing mutations. *Neuron*, **81**, 536–543.
22. Coyne, A.N., Siddegowda, B.B., Estes, P.S., Johannesmeyer, J., Kovalik, T., Daniel, S.G., Pearson, A., Bowser, R. and Zarnescu, D.C. (2014) Futsch/MAP1B mRNA Is a translational target of TDP-43 and is neuroprotective in a Drosophila model of amyotrophic lateral sclerosis. *J. Neurosci.*, **34**, 15962–15974.
23. Cushman, M., Johnson, B.S., King, O.D., Gitler, A.D. and Shorter, J. (2010) Prion-like disorders: blurring the divide between transmissibility and infectivity. *J. Cell Sci.*, **123**, 1191–1201.
24. King, O.D., Gitler, A.D. and Shorter, J. (2012) The tip of the iceberg: RNA-binding proteins with prion-like domains in neurodegenerative disease. *Brain Res.*, **1462**, 61–80.
25. Ou, S.H., Wu, F., Harrich, D., Garcia-Martinez, L.F. and Gaynor, R.B. (1995) Cloning and characterization of a novel cellular protein, TDP-43, that binds to human immunodeficiency virus type 1 TAR DNA sequence motifs. *J. Virol.*, **69**, 3584–3596.
26. Voigt, A., Herholz, D., Fiesel, F.C., Kaur, K., Muller, D., Karsten, P., Weber, S.S., Kahle, P.J., Marquardt, T. and Schulz, J.B. (2010) TDP-43-mediated neuron loss in vivo requires RNA-binding activity. *PLoS One*, **5**, e12247.
27. Ihara, R., Matsukawa, K., Nagata, Y., Kunugi, H., Tsuji, S., Chihara, T., Kuranaga, E., Miura, M., Wakabayashi, T., Hashimoto, T. *et al.* (2013) RNA binding mediates neurotoxicity in the transgenic Drosophila model of TDP-43 proteinopathy. *Hum. Mol. Genet.*, **22**, 4474–4484.
28. Freibaum, B.D., Chitta, R.K., High, A.A. and Taylor, J.P. (2010) Global analysis of TDP-43 interacting proteins reveals strong association with RNA splicing and translation machinery. *J. Proteome Res.*, **9**, 1104–1120.
29. Fallini, C., Bassell, G.J. and Rossoll, W. (2012) The ALS disease protein TDP-43 is actively transported in motor neuron axons and regulates axon outgrowth. *Hum. Mol. Genet.*, **21**, 3703–3718.
30. Wang, I.F., Wu, L.S., Chang, H.Y. and Shen, C.K. (2008) TDP-43, the signature protein of FTLD-U, is a neuronal activity-responsive factor. *J. Neurochem.*, **105**, 797–806.
31. Yu, Z., Fan, D., Gui, B., Shi, L., Xuan, C., Shan, L., Wang, Q., Shang, Y. and Wang, Y. (2012) Neurodegeneration-associated TDP-43 interacts with fragile X mental retardation protein (FMRP)/Staufen (STAU1) and regulates SIRT1 expression in neuronal cells. *J. Biol. Chem.*, **287**, 22560–22572.
32. Colombrita, C., Zennaro, E., Fallini, C., Weber, M., Sommacal, A., Buratti, E., Silani, V. and Ratti, A. (2009) TDP-43 is recruited to stress granules in conditions of oxidative insult. *J. Neurochem.*, **111**, 1051–1061.
33. Dewey, C.M., Cenik, B., Sephton, C.F., Dries, D.R., Mayer, P. III, Good, S.K., Johnson, B.A., Herz, J. and Yu, G. (2011) TDP-43 is directed to stress granules by sorbitol, a novel physiological osmotic and oxidative stressor. *Mol. Cell. Biol.*, **31**, 1098–1108.
34. McDonald, K.K., Aulas, A., Destroismaisons, L., Pickles, S., Beleac, E., Camu, W., Rouleau, G.A. and Vande Velde, C. (2011) TAR DNA-binding protein 43 (TDP-43) regulates stress granule dynamics via differential regulation of G3BP and TIA-1. *Hum. Mol. Genet.*, **20**, 1400–1410.
35. Liu-Yesucevitz, L., Bilgutay, A., Zhang, Y.J., Vanderwyde, T., Citro, A., Mehta, T., Zaarur, N., McKee, A., Bowser, R., Sherman, M. *et al.* (2010) Tar DNA binding protein-43 (TDP-43) associates with stress granules: analysis of cultured cells and pathological brain tissue. *PLoS ONE*, **5**, e13250.

36. Estes, P.S., Daniel, S.G., McCallum, A.P., Boehringer, A.V., Sukhina, A.S., Zwick, R.A. and Zarnescu, D.C. (2013) Motor neurons and glia exhibit specific individualized responses to TDP-43 expression in a Drosophila model of amyotrophic lateral sclerosis. *Dis. Model. Mech.*, **6**, 721–733.
37. Parker, S.J., Meyerowitz, J., James, J.L., Liddell, J.R., Crouch, P.J., Kanninen, K.M. and White, A.R. (2012) Endogenous TDP-43 localized to stress granules can subsequently form protein aggregates. *Neurochem. Int.*, **60**, 415–424.
38. Ramaswami, M., Taylor, J.P. and Parker, R. (2013) Altered ribostasis: RNA-protein granules in degenerative disorders. *Cell*, **154**, 727–736.
39. Wolozin, B. (2012) Regulated protein aggregation: stress granules and neurodegeneration. *Mol. Neurodegener.*, **7**, 56.
40. Li, Y.R., King, O.D., Shorter, J. and Gitler, A.D. (2013) Stress granules as crucibles of ALS pathogenesis. *J. Cell Biol.*, **201**, 361–372.
41. Liu-Yesucevitz, L., Bassell, G.J., Gitler, A.D., Hart, A.C., Klann, E., Richter, J.D., Warren, S.T. and Wolozin, B. (2011) Local RNA translation at the synapse and in disease. *J. Neurosci.*, **31**, 16086–16093.
42. Callan, M.A., Clements, N., Ahrendt, N. and Zarnescu, D.C. (2012) Fragile X Protein is required for inhibition of insulin signaling and regulates glial-dependent neuroblast reactivation in the developing brain. *Brain Res.*, **1462**, 151–161.
43. Elden, A.C., Kim, H.J., Hart, M.P., Chen-Plotkin, A.S., Johnson, B.S., Fang, X., Armakola, M., Geser, F., Greene, R., Lu, M.M. *et al.* (2010) Ataxin-2 intermediate-length polyglutamine expansions are associated with increased risk for ALS. *Nature*, **466**, 1069–1075.
44. Nonaka, T., Masuda-Suzukake, M., Arai, T., Hasegawa, Y., Akatsu, H., Obi, T., Yoshida, M., Murayama, S., Mann, D.M., Akiyama, H. *et al.* (2013) Prion-like properties of pathological TDP-43 aggregates from diseased brains. *Cell Rep.*, **4**, 124–134.
45. Zhang, Y.Q., Bailey, A.M., Matthies, H.J., Renden, R.B., Smith, M.A., Speese, S.D., Rubin, G.M. and Broadie, K. (2001) Drosophila fragile X-related gene regulates the MAP1B homolog Futsch to control synaptic structure and function. *Cell*, **107**, 591–603.
46. Kim, H.J., Raphael, A.R., Ladow, E.S., McGurk, L., Weber, R.A., Trojanowski, J.Q., Lee, V.M., Finkbeiner, S., Gitler, A.D. and Bonini, N.M. (2014) Therapeutic modulation of eIF2alpha phosphorylation rescues TDP-43 toxicity in amyotrophic lateral sclerosis disease models. *Nat. Genet.*, **46**, 152–160.
47. Smith, B.N., Ticozzi, N., Fallini, C., Gkazi, A.S., Topp, S., Kenna, K.P., Scotter, E.L., Kost, J., Keagle, P., Miller, J.W. *et al.* (2014) Exome-wide rare variant analysis identifies TUBA4A mutations associated with familial ALS. *Neuron*, **84**, 324–331.
48. He, F., Krans, A., Freibaum, B.D., Taylor, J.P. and Todd, P.K. (2014) TDP-43 suppresses CGG repeat-induced neurotoxicity through interactions with HnRNP A2/B1. *Hum. Mol. Genet.*, **23**, 5036–5051.
49. Galloway, J.N., Shaw, C., Yu, P., Parghi, D., Poidevin, M., Jin, P. and Nelson, D.L. (2014) CGG repeats in RNA modulate expression of TDP-43 in mouse and fly models of fragile X tremor ataxia syndrome. *Hum. Mol. Genet.*, **23**, 5906–5915.
50. Gustafson, K. and Boulianne, G.L. (1996) Distinct expression patterns detected within individual tissues by the GAL4 enhancer trap technique. *Genome*, **39**, 174–182.
51. Estes, P.S., O'Shea, M., Clasen, S. and Zarnescu, D.C. (2008) Fragile X protein controls the efficacy of mRNA transport in Drosophila neurons. *Mol. Cell. Neurosci.*, **39**, 170–179.
52. Cassel, J.A., Blass, B.E., Reitz, A.B. and Pawlyk, A.C. (2010) Development of a novel nonradiometric assay for nucleic acid binding to TDP-43 suitable for high-throughput screening using AlphaScreen technology. *J. Biomol. Screen.*, **15**, 1099–1106.
53. Cassel, J.A., McDonnell, M.E., Velvadapu, V., Andrianov, V. and Reitz, A.B. (2012) Characterization of a series of 4-aminoquinolines that stimulate caspase-7 mediated cleavage of TDP-43 and inhibit its function. *Biochimie*, **94**, 1974–1981.
54. Pfaffl, M.W. (2001) A new mathematical model for relative quantification in real-time RT-PCR. *Nucleic Acids Res.*, **29**, e45.